Membrane docking of the C2 domain from protein kinase Cα as seen by polarized ATR-IR. The role of PIP$_2$

Alessio Ausili [a], Senena Corbalán-García [a], Juan C. Gómez-Fernández [a,*], Derek Marsh [b,*]

[a] Departamento de Bioquímica y Biología Molecular A, Universidad de Murcia, Apartado 4021, 30080-Murcia, Spain
[b] Max-Planck-Institut für biophysikalische Chemie, Abt. Spektroskopie, 37070 Göttingen, Germany

ABSTRACT

We have used attenuated total internal reflection infrared spectroscopy (ATR-IR) spectroscopy to study the association of the C2 domain from protein kinase Cα (PKCα) with different phospholipid membranes, so as to characterise the mode of membrane docking and its modulation by the second-messenger lipid PIP$_2$. In parallel, we have also examined the membrane interaction of the C2 domain from cytosolic phospholipase A$_2$. PIP$_2$ did not induce significant changes in secondary structure of the membrane-bound PKCα-C2 domain, nor did binding of the PKCα-C2 domain change the dichroic ratios of the lipid chains, whereas the C2 domain from phospholipase A$_2$ did perturb the lipid chain orientation. Measurements of the dichroic ratios for the amide I and amide II protein bands were combined so as to distinguish the tilt of the β-sheets from that of the β-strands within the sheet. When associated with POPC/POPS membranes, the β-sandwich of the PKCα-C2 domain is inclined at an angle α = 35° to the membrane normal, i.e., is oriented more nearly perpendicular than parallel to the membrane. In the process of membrane docking, the tilt angle increases to α = 44° in the presence of PIP$_2$, indicating that the β-sandwich comes closer to the membrane surface, so confirming the importance of this lipid in determining docking of the C2 domain and consequent activation of PKCα.

© 2010 Elsevier B.V. All rights reserved.

1. Introduction

Protein kinase C (PKC) composes a large family of phospholipid-dependent serine/threonine kinases, which are activated by many extracellular signals and play a critical role in several signalling pathways within the cell [1–3]. PKC is involved in a multiplicity of cellular functions and processes, from control of fundamental cell-autonomous activities, such as proliferation, modulation of structural membrane events, and regulation of transcription and cell growth, to higher functions of the organism, such as learning and memory [4]. The mammalian isoenzymes have been grouped into three subfamilies according to their enzymatic properties: classical, novel and atypical [4,5]. The first group comprises the classical isoenzymes (cPKCs), including PKCα, PKCβI, PKCβII and PKCγ, which exhibit conserved C1 and C2 regulatory domains. These isoenzymes are regulated by diacylglycerol (DAG) and, cooperatively, also by Ca^{2+} and acidic phospholipids.

All C2 domains share a common overall fold: a single compact Greek-key motif consisting of eight antiparallel β-strands assembled in a β-sandwich with flexible loops on top and at the bottom of the sandwich [3,6]. This C2-domain architecture displays two functional motifs. The first is the Ca^{2+}-binding region, which is located in the flexible upper loops, binds two or three Ca^{2+} ions, depending on the isoenzyme, and also interacts with phosphatidylserine (PS) [7–11]. The second site is located in a groove formed by strands β3 and β4. This was found to be an additional binding site for anionic phospholipids, when the three-dimensional structure of the domain bound to soluble phospholipids was first determined [9,12] and also a site where other molecules like retinoic acid may also bind [13]. Moreover, several studies based on crystallographic, biochemical, and cell biology approaches have shown that this site exhibits a high specificity for the second-messenger lipid PIP$_2$ [14–20].

Extensive biochemical studies have been undertaken to assess the role of both regulatory sites in the localization and activation of full-length PKCα. Site-directed mutagenesis, performed for each motif, has shed light on their differential lipid binding affinities. Substitution of key Asp residues in the Ca^{2+}-binding region by Asn leads to complete loss of lipid binding and catalytic activity [11,21,22]. Different extents of inhibition were found when the residues

responsible for direct interaction with PS were mutated, confirming that these sites also contribute to anchor the domain to the membrane, where the main role is played by Ca^{2+} that acts as a bridge connecting the top of the C2 domain with the lipid surface [10,21]. Interestingly, mutants with the Ca^{2+}/PS region disabled still retain their ability to bind to PIP_2-containing vesicles, although with slightly lower affinity [9,14–17]. In contrast, mutations that knock-down the β-groove do not affect the Ca^{2+}/PS binding but completely abolish the PIP_2 interaction [9,14–17]. Together, these results indicate that Ca^{2+} is always needed to dock the domain to the membrane and, while PS targets the domain by interacting with the Ca^{2+}-binding region, PIP_2 targets the domain by interacting with the β-groove.

The existence of two distinct binding sites in the C2 domains of cPKCs suggests that they may function in ways not described so far, because these proteins could well be activated in a PS- and/or PIP_2-dependent manner. In order to verify the physiological importance of these capacities of the C2 domain, a number of *in vivo* studies have been carried out. Studies in different cell models show that the β-groove is essential for membrane docking, independent of the level of DAG generated by PIP_2 hydrolysis [15–20]. In addition, several approaches to increase the PIP_2 concentration available at the plasma membrane have shown enhanced retention of PKCα docked in this area, increasing the half-maximal dissociation time [15,20,23].

Also of interest for understanding how PIP_2 can contribute to activation of cPKCs, is the observation that PIP_2 decreases the Ca^{2+} requirement for membrane binding of the C2 domain [17–19]. This is especially the case for PKCα, which exhibits the lowest Ca^{2+} requirement, followed by PKCγ and PKCβ [18,19]. Most importantly, this also correlates with retention of each domain at the plasma membrane of PC12 cells upon stimulation by ATP [19], indicating that local concentrations of the target lipids PS and PIP_2 on the inner leaflet of the plasma membrane are sufficient to drive Ca^{2+}-activated membrane docking during physiological stimulation.

The 3D structure of the C2 domain of PKCα complexed with Ca^{2+}, PS and PIP_2 clearly shows that PS interacts with the Ca^{2+}-binding region and that PIP_2 interacts with the β-groove [18]. Notably, there is a concentration of cationic and aromatic residues in the β-groove that establishes direct interactions with the phosphate moieties of the inositol ring [18]. In fact, substitution of the aromatic residues, to abolish their interaction with phosphoinositide, severely impairs the ability of PKCα to translocate from the cytosol to the plasma membrane in PC12 cells stimulated with ATP [18]. More importantly, enzyme function is not recovered by addition of excess Ca^{2+} and DAG, suggesting that interaction of the C2 domain with the plasma membrane is a key event in localizing the enzyme to its proper compartment, through interaction with the target lipids.

Docking of the C2 domain on membranes is, therefore, crucial to the way in which the two binding motifs interact with their target lipids. Previously, studies on PKCα-C2 and other C2 domains have been carried out by using site-directed spin-label EPR, in conjunction with relaxation enhancement agents that preferentially localise either to the aqueous phase or to the membrane [24–26]. For PKCα-C2 it was concluded that the domain docked in a nearly parallel orientation with respect to the plasma membrane surface, consistent with the X-ray crystal structure determined in the presence of water-soluble anionic lipids [8,9,24]. Very recently, however, this conclusion has been questioned, based on measurements of X-ray reflectivity for the PKCα-C2 domain bound to lipid monolayers [27].

Both site-directed EPR with relaxation agents and X-ray reflectivity are essentially depth-dependent, not angular, measurements. Thus, it seems desirable to investigate the membrane docking of C2 domains by using a method that is directly sensitive to angular orientation. Measurement of infrared dichroism on aligned samples (see, e.g., ref. [28]) is one such approach. In the form of attenuated total internal reflection infrared spectroscopy (ATR-IR), this technique has been successfully applied to study α-helical proteins (see, e.g.,

refs. [29–33]), and also β-sheet and β-barrel proteins (see, e.g., refs. [34–42]), but so far no studies have been carried out on β-sandwich structures such as C2 domains.

In the present work, we use polarized ATR-IR as a new procedure to study the molecular docking of C2 domains from PKCα to POPC membranes that contain the anionic target lipids POPS or POPA. Particular emphasis is put on studying the influence of PIP_2 on the docking orientation. To achieve this, a previous treatment of IR-dichroism for isolated β-sheets [36] is extended to include β-sandwich structures. In this way, both the inclination of the β-sandwich to the membrane and the tilt of the β-strands within the β-sheets can be determined. In order to compare with a further C2 domain for which docking studies have been undertaken with site-directed EPR [26], we also apply the method to study the binding of the C2 domain from cytosolic phospholipase A_2 (cPLA$_2$-C2) to POPC/POPS membranes.

2. Materials and methods

2.1. Materials

1-Palmitoyl-2-oleoyl-*sn*-glycero-3-phosphocholine (POPC), 1-palmitoyl-2-oleoyl-*sn*-glycero-3-(phospho-L-serine) (POPS), 1-palmitoyl-2-oleoyl-*sn*-glycero-3-phosphate (POPA) and L-α-phosphatidylinositol-4,5-bisphosphate (PIP_2) were purchased from Avanti Polar Lipids (Alabaster, AL, USA). Deuterium oxide (99.9% D_2O) was purchased from Aldrich (Madrid, Spain). All other reagents and solvents were commercial samples of the highest purity. The PKCα-C2 domain and the cPLA$_2$-C2 domain were expressed and purified as described by Torrecillas et al. [43] and Nalefski et al. [44], respectively.

2.2. Sample preparation for ATR-IR measurements

Solutions of 2 μmol of POPC/POPS (75:25 molar ratio), POPC/POPA (75:25 molar ratio), POPC/POPS/PIP_2 (70:25:5 molar ratio) and POPC/POPA/PIP_2 (70:25:5 molar ratio) lipid mixtures were used to prepare multilamellar liposomes (MLVs). The lipids dissolved in chloroform were dried with N_2 flow [45]. Last traces of solvent were removed by a further 2 h under high vacuum. MLVs were generated by hydrating with buffer containing 20 mM Hepes, 100 mM KCl pH 7.5 and vortexing vigorously. Then $CaCl_2$ was added to a final concentration of 1 mM, and PKCα-C2 domain or cPLA$_2$-C2 domain was added to obtain a final protein concentration of 0.06 μM. Samples were incubated for 20 min at 25 °C, and then unbound protein in the supernatant was removed by centrifugation. Oriented thick multilayer films were obtained by applying the protein-bound lipid dispersions directly onto a germanium ATR plate, followed by drying under a stream of oxygen-free N_2 gas. Protein-free bilayer preparations of POPC/POPS or POPC/POPS/PIP_2 were subject to an identical treatment. In order to render the germanium plate hydrophilic, it was previously washed with alkaline detergent, rinsed with deionized water and finally washed with methanol and chloroform. The membrane-bearing ATR-plate was placed in the liquid sample holder and spectra of the dry sample were recorded. Then the liquid sample holder was connected to an air stream (saturated with D_2O) and the sample was hydrated for at least 2 h. Spectra of the hydrated sample were then recorded. The spectra of both dry and hydrated samples were collected at 25 °C, with the incident radiation polarized parallel and perpendicular relative to the plane of incidence.

2.3. ATR-IR spectroscopy

ATR spectra were recorded on a Bruker Vector 22 Fourier-transform infrared spectrometer equipped with a liquid-nitrogen-cooled MCT detector and using a germanium ATR plate (Specac, Orpington, U.K.) (52 mm × 20 mm × 2 mm) with an aperture angle of 45° as internal reflection element. Spectra were recorded with parallel

and perpendicular polarization of the incident beam by using a ZnSe polarizer (Specac, Orpington, U.K.) at room temperature. According to the specifications of the manufacturer, the degree of polarization in the relevant region of the mid-IR is 99% and therefore likely to contribute negligibly to the uncertainty in dichroic ratio. Resettability of the polarizer angle (around ± 1° at most) is included in the random error and unlikely to be a significant contributor.

A total of 128 scans were averaged for each spectrum with a nominal resolution of 4 cm^{-1}. At least 24 h before and during data acquisition, the spectrometer was purged continuously with dry air. Remaining interference from water vapour absorption was eliminated by subtracting a separately measured water vapour spectrum from the original spectra. Finally, spectra were smoothed with a 9-point Savitsky–Golay filter to remove further noise from residual water vapour. Before every experiment, background single-beam spectra were collected with the clean ATR crystal alone. Then, the samples were oriented on the germanium plate, as described above, and ATR-absorbance spectra of the dry and hydrated sample were collected, in conjunction with the previously recorded background spectra. Because POPS absorbs in the amide I region, spectra of the POPS-containing lipid mixtures were recorded in the absence of protein, and these were subtracted from the spectra of samples containing bound protein. Note that, when POPA (which has no background signal in the amide I region) is used as a surrogate negatively charged lipid in place of POPS, the results obtained are qualitatively similar to those deduced for POPS after background subtraction.

Polarized ATR spectra of the hydrated samples were used to calculate the secondary structure composition of the PKCα-C2 domain. Spectra were processed using Opus-NT 2.0 software from Bruker. Band decomposition and estimation of the secondary structure composition were performed as described [46], by using the peak-picking module based on smoothed second-derivative spectra that is included in OriginPro 7.5 software (OriginLab Corp., Northampton, MA), followed by two-stage curve fitting with Gaussian peaks. In the first stage, peak positions were fixed and intensities and widths were optimised; in the second stage, the positions were also released to produce fine-tuning in the final optimisation. The nonlinear least-squares optimisation routine used for fitting the bandshapes in OriginPro 7.5 is based on the Levenberg–Marquardt algorithm. Dichroic ratios were determined from the integrated areas of the polarized spectra. Specifically, areas assigned to the principal β-sheet absorptions of the amide I and amide II bands were used to obtain R_I (amide I) and R_{II} (amide II), those of the CH$_2$ symmetric and antisymmetric stretching bands to obtain $R_{CH_2}(2850)$ and $R_{CH_2}(2920)$, respectively, and that of the lipid carbonyl band to approximate R_{ISO}. Identical input band-fitting components were used for both parallel and perpendicular polarizations. Mean values and standard deviations were calculated from triplicate experiments under the same conditions and with the same parameter settings. The ratios of the components of the electric field intensities of the evanescent infrared wave used for interpretation of dichroic ratios and estimation of secondary structure content are: $E_x^2/E_y^2 = 0.853$ (0.877) and $E_z^2/E_y^2 = 1.147$ (0.828), for a 45°-cut germanium ATR plate in the thick (thin) film approximation (see, e.g., ref. [28]).

Note that, in order to minimize random errors in comparing the effects of different lipids — especially PIP$_2$, a standardized protocol was used throughout for sample preparation and handling, and for spectral data collection and fitting.

3. Results

3.1. Secondary structure

Fig. 1 shows the amide I region from the ATR-IR absorbance spectra (top) and second derivative spectra (bottom) of the PKCα-C2 domain in the presence of hydrated POPC/POPS (panel A) and POPC/

POPS/PIP$_2$ (panel B) membranes. These spectra are quite similar to those obtained from previous FTIR analyses [22,43]. This indicates that the secondary structure was not affected by the procedures used to align the membranes on the surface of the ATR crystal. The apparent positions registered by the second-derivative spectra are shifted from the true positions that are fitted to the original absorption spectra, because of overlap between the component bands. The second-derivative positions were used as initial estimates in the band fitting, and these were subsequently refined in the fitting process (which allows for the effects of overlap). As far as possible, consistent band-fitting components were used throughout and across the different analyses, also for determining the dichroic ratios (see below). To exclude the possibility of any irreversible effects on the protein during drying the sample on the ATR surface, the protein was re-dissolved in buffer after drying and its functionality was assayed by monitoring binding affinity to phospholipid vesicles at different lipid concentrations, as described previously [47]. Results (not shown) were identical, to within experimental error, with those for protein that had not been subject to this drying procedure.

The bands obtained after fitting the absorption spectrum can be attributed to the following secondary structural elements, which are based on consensus data established for proteins hydrated in D$_2$O [48]: β-sheet (1634 cm^{-1}), α-helix (1649 cm^{-1}), β-turns (1661 cm^{-1}), unordered structures and/or loops (1643 cm^{-1}). The band at 1679 cm^{-1} can be assigned to antiparallel β-sheet, while the 1690 cm^{-1} band is of less certain origin because both β-turns and aggregated β-sheet can contribute in this spectral region [49]. The bands below 1620 cm^{-1} are due to amino acid side chain absorptions [50]. Comparison of the PKCα-C2 domain spectrum in the absence of PIP$_2$ with that in its presence does not show significant changes; only tiny changes are detected in the difference spectrum, demonstrating no – or very small – differences in secondary structure. Also when POPA was used instead of POPS, analysis of the ATR-IR spectra did not show important changes in secondary structure of the PKCα-C2 domain, both in the presence and absence of PIP$_2$ (spectra not shown).

In order to estimate the secondary structure content for oriented samples, a combination of band fittings from parallel and perpendicular polarized spectra must be performed [46]. Fig. 2 shows, as an example, curve fitting of the amide I band of the PKCα-C2 domain in the absence (top panels) and presence (bottom panels) of PIP$_2$ in the lipid membrane. The band areas from parallel (A$_{//}$) and perpendicular (A$_\perp$) polarized radiations are combined according to the following equation:

$$A = A_{//} + G \times A_\perp \tag{1}$$

where $G \equiv 2\frac{E_z^2}{E_y^2} - \frac{E_x^2}{E_y^2} = 1.441$, for the thick film approximation and a 45°-cut Ge ATR crystal [46]. The secondary structure contents that are derived in this way for the PKCα-C2 domain associated with different lipid membranes are given in Table 1. Note that the standard deviations given in Table 1 include contributions to the measured random error from the uncertainties in band fitting.

When POPS was used as the anionic lipid component in the membrane, the additional presence of PIP$_2$ did not affect the secondary structure of the PKCα-C2 domain (Table 1). Most of the small differences observed can be attributed to measurement and fitting errors. Both sets of spectra show β-sheet as the major component: it represents about 50% of the total band area. The bands from α-helix, and the unordered structures and/or loops contribute 11% and 10% respectively, while the band assigned to β-turns constitutes about 20% of the total intensity. Finally, the bands at 1676 cm^{-1} and 1690 cm^{-1} represent 6% and 2% contributions, respectively. Very similar results were obtained when POPS was replaced by POPA as the anionic target lipid. As shown in Table 1, the only changes are a small decrease in the β-sheet band area and concomitant increase in the β-turn band area, in the presence of PIP$_2$,
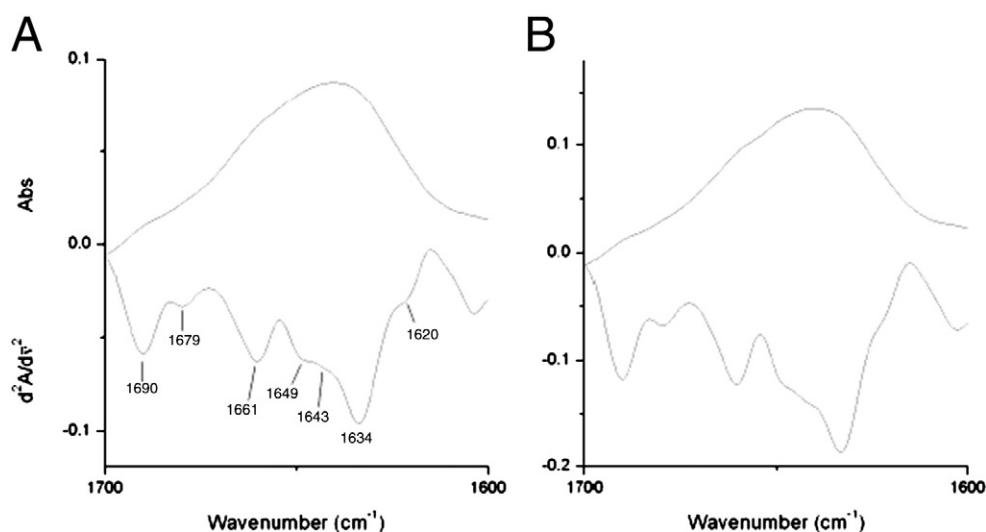
Fig. 1. Amide I region in the absorption (top) and second-derivative (bottom) ATR-IR spectra of the PKCα-C2 domain associated with POPC membranes containing 25 mol% POPS, without (A) and with (B) 5 mol% PIP$_2$.

although this is within the uncertainty range. Correspondingly, band fitting of polarized ATR-IR spectra from the cPLA$_2$-C2 domain in the presence of POPC/POPS membranes was also performed. In this case, a further band is present close to 1626 cm^{-1} that can be assigned to β-strands which are particularly exposed to solvent [51]. Nonetheless, the predominant component of the secondary structure is, as expected [52], the β-strands which represent about 50% of the total, whereas the contribution from α-helix is only about 5%. The secondary structural content of the cPLA$_2$-C2 domain associated with POPC/POPS membranes is summarized also in Table 1.

3.2. Lipid chain orientation

Fig. 3 (left side) shows the CH$_2$-stretch region in the polarized ATR-IR spectra and dichroic difference spectra from dry samples of POPC/POPS, with and without PIP$_2$, in the presence of the PKCα-C2 domain. The bands close to 2920 cm^{-1} (antisymmetric CH$_2$ stretching band) and

2850 cm^{-1} (symmetric CH$_2$ stretching band) were used to assess the lipid acyl chain ordering. A positive or a negative peak in the dichroic difference spectra indicates a preferential orientation of the transition moment relative to the ATR plate, whereas a flat baseline results in the absence of any preferential orientation [53]. The transition moments for methylene stretch vibrations lie in the plane of the C–H bonds, which is perpendicular to the lipid chain axis. Therefore, a negative dichroism implies a chain orientation preferentially parallel to the normal to the ATR plate. In the case of POPC/POPS, the difference dichroic spectra show negative deviations at the wave numbers corresponding to the CH$_2$ stretching bands, indicating ordering relative to the membrane normal. A chain order parameter can be determined from the corresponding dichroic ratios, R_{CH_2} (see, e.g., refs. [30,31]):

$$\langle P_2(\cos\theta_{ch}) \rangle = \frac{2\left(E_z^2/E_y^2 + E_x^2/E_y^2 - R_{CH_2}\right)}{2E_z^2/E_y^2 - E_x^2/E_y^2 + R_{CH_2}} \tag{2}$$
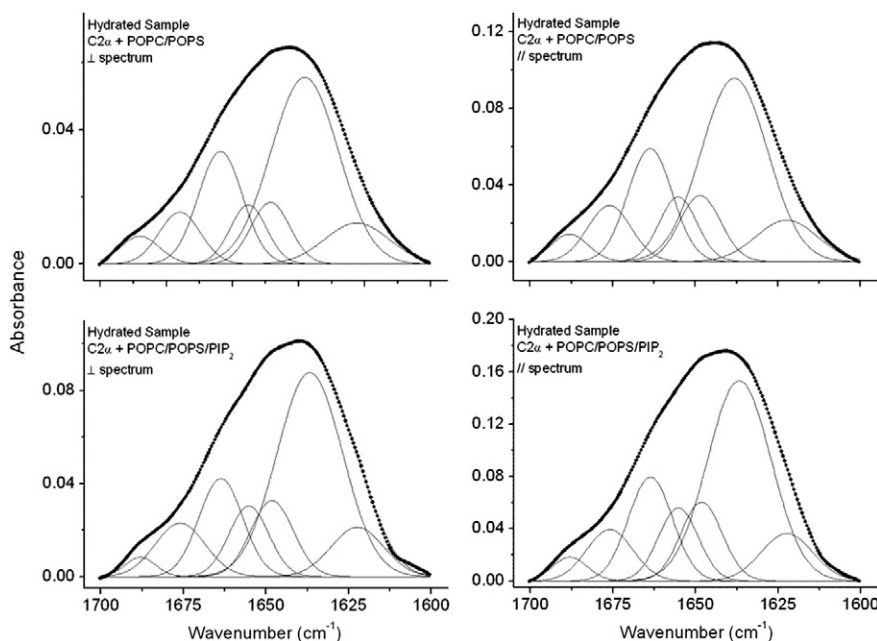

Fig. 2. Amide I absorbance band contours (symbols), together with the best fitting Gaussian individual components (lines), for hydrated samples of PKCα-C2 domain docked with POPC membranes containing 25 mol% POPS, with (bottom) and without (top) 5 mol% PIP$_2$. Band fitting is performed for ATR-IR spectra recorded with parallel (right) and perpendicular (left) polarized radiation.

Table 1
Secondary structure content of PKCα-C2 and cPLA₂ domains bound to POPC membranes containing 25 mol% POPS or POPA, with and without 5 mol% PIP₂.

PKCα-C2 POPC/POPS		PKCα-C2 POPC/POPS/PIP₂		PKCα-C2 POPC/POPA		PKCα-C2 POPC/POPA/PIP₂		cPLA₂-C2 POPC/POPS	
Centre (cm^{-1})	Fitting (%)	Centre (cm^{-1})	Fitting (%)	Centre (cm^{-1})	Fitting (%)	Centre (cm^{-1})	Fitting (%)	Centre (cm^{-1})	Fitting (%)
								1626	15.9 ± 2.4
1638	50.0 ± 6.6	1637	50.4 ± 1.7	1639	49.8 ± 3.5	1637	45.6 ± 3.7	1637	33.7 ± 2.2
1649	10.6 ± 0.6	1648	10.5 ± 5.2	1649	9.6 ± 2.5	1648	9.9 ± 4.7	1648	13.2 ± 3.7
1655	10.5 ± 2.8	1655	11.5 ± 1.6	1655	12.3 ± 2.3	1654	12.0 ± 2.7	1655	5.2 ± 1.8
1664	20.0 ± 4.8	1664	19.0 ± 4.3	1663	20.4 ± 2.4	1663	21.9 ± 6.7	1664	15.9 ± 3.2
1676	6.3 ± 2.4	1676	6.2 ± 2.8	1677	7.2 ± 2.3	1676	7.8 ± 3.8	1676	12.9 ± 2.5
1688	2.6 ± 1.3	1688	2.4 ± 0.3	1689	0.7 ± 0.9	1691	2.8 ± 2.8	1687	3.3 ± 1.3

Mean values and standard deviations ($\pm$ sd) were calculated from triplicate experiments.

where angular brackets indicate an ensemble average. Alternatively, the chain order can be expressed by an effective net tilt of the chains, θ_{eff}, which is derived from the order parameter: $\langle P_2(\cos\theta_{ch})\rangle = \frac{1}{2}(3\cos^2\theta_{eff} - 1)$, by assuming a singular distribution. For unhydrated POPC/POPS membranes it is calculated that the lipid chains make an effective angle of $\theta_{eff} = 30 \pm 3°$ with the ATR plate normal, corresponding to an order parameter of $\langle P_2(\cos\theta_{ch})\rangle = 0.62 \pm 0.06$, indicating that the POPC/POPS membrane is well ordered. Further, the presence of PIP₂ does not affect the chain order appreciably (the order parameter is 0.61 ± 0.07 corresponding to an effective tilt of $31 \pm 3°$). Somewhat lower chain order is obtained when POPS is replaced by POPA: $\langle P_2(\cos\theta_{ch})\rangle = 0.50 \pm 0.05$ and $\theta_{eff} = 35 \pm 2°$ in the absence of PIP₂, but this does not change significantly in the presence of PIP₂: $\langle P_2(\cos\theta_{ch})\rangle = 0.53 \pm 0.08$ and $\theta_{eff} = 34 \pm 3°$. Little change in lipid chain

ordering is observed on interaction with the C2 domain from PKCα, but a change in chain order occurs when the cPLA₂-C2 domain associates with lipid membranes (see Table 2). In the latter case, the acyl chain order of POPC/POPS membranes increases to $\langle P_2(\cos\theta_{ch})\rangle = 0.73 \pm 0.05$, corresponding to an effective angle of $\theta_{eff} = 25 \pm 3°$ with the normal to the ATR plate. When the samples are hydrated, it is observed that the membranes remain ordered with effective chain tilts around 34°. All dichroic ratios, order parameters and effective tilt angles of the lipid chains are reported in Table 2.

3.3. Orientation of C2 domains docked to membranes

Fig. 4 shows the amide and carbonyl regions of the ATR-IR spectra with parallel and perpendicular polarizations of the incident radiation,
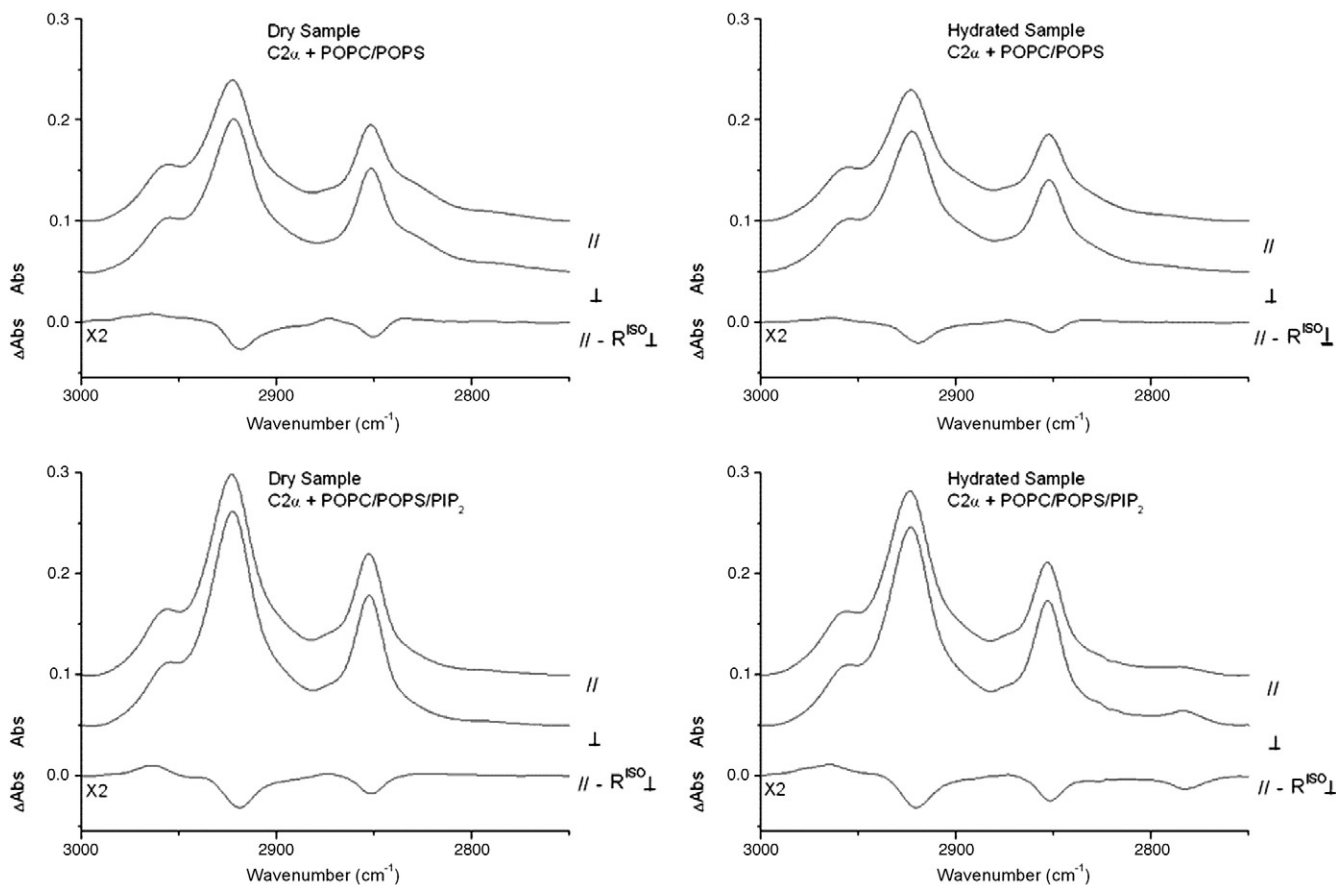

Fig. 3. CH₂-stretch region in the ATR-IR spectra from dry (left) and hydrated (right) samples of the PKCα-C2 domain in the presence of 75:25 mol/mol POPC/POPS (top) and 70:25:5 mol/mol/mol POPC/POPS/PIP₂ (bottom) membranes, for parallel (//, upper spectra) and perpendicular (⊥, middle spectra) polarized radiation. The dichroic difference spectra ($A_{//} - R_{iso}A_{\perp}$, lower spectra) are obtained by subtracting the perpendicular-polarized spectra from the parallel-polarized spectra, after multiplication of the perpendicular-polarized spectra by the dichroic ratio, R_{iso}, appropriate to an isotropic sample distribution. R_{iso} is approximated by the dichroic ratio of the lipid carbonyl band (see Fig. 4), assumed to correspond to orientation at the magic angle [67]. The spectra are shown in the 3000–2750 cm^{-1} region and are shifted vertically but have the same vertical scale.

Table 2
Dichroic ratio (R_{CH_2}), order parameter ($\langle P_2(\cos\theta_{ch})\rangle$) and effective tilt angle (θ_{eff}) of lipid chains in aligned membranes of POPC containing 25 mol% POPS or POPA, with and without 5 mol% PIP$_2$, in the presence of PKCα- or cPLA$_2$-C2 domain.

Dichroic ratio, order parameter and effective tilt	PKCα-C2 POPC/POPS		PKCα-C2 POPC/POPS/PIP$_2$		PKCα-C2 POPC/POPA		PKCα-C2 POPC/POPA/PIP$_2$		cPLA$_2$-C2 POPC/POPS	
	Dry	Hydrated	Dry	Hydrated	Dry	Hydrated	Dry	Hydrated	Dry	Hydrated
R_{CH_2}	1.40 ± 0.04	1.50 ± 0.05	1.40 ± 0.05	1.46 ± 0.05	1.49 ± 0.04	1.47 ± 0.01	1.46 ± 0.06	1.46 ± 0.05	1.32 ± 0.04	1.42 ± 0.06
$\langle P_2(\cos\theta_{ch})\rangle$	0.62 ± 0.06	0.49 ± 0.06	0.61 ± 0.07	0.54 ± 0.06	0.50 ± 0.05	0.53 ± 0.01	0.53 ± 0.08	0.53 ± 0.06	0.73 ± 0.05	0.59 ± 0.08
θ_{eff} (°)	30 ± 3	36 ± 3	31 ± 3	34 ± 3	35 ± 2	34 ± 1	34 ± 3	34 ± 3	25 ± 3	31 ± 3

Mean values and standard deviations ($\pm$sd) were calculated from triplicate experiments and deduced from the dichroism of both the CH$_2$ antisymmetric (2920 cm^{-1}) and symmetric (2850 cm^{-1}) stretching bands.

and the corresponding dichroic spectra, for the PKCα-C2 domain bound to POPC/POPS membranes, with and without PIP$_2$. Both the amide I band centred at around 1650 cm^{-1} and the amide II band centred at around 1540 cm^{-1} are visible for the samples dried from H$_2$O. For samples hydrated in D$_2$O, however, the amide II band of the deuterated protein is shifted to lower wave numbers, into regions of spectral overlap. Dichroic ratios of the amide I and amide II bands for dry samples, and of the amide I band for hydrated samples, are given in the upper rows of Table 3. Data are presented for the PKCα-C2 domain bound to membranes of different lipid compositions, and also for the cPLA$_2$-C2 domain bound to POPC/POPS membranes.

The IR-dichroism of membrane-bound β-sheets and β-barrels has been treated previously [36–38]. The orientation of a flat (i.e., non-twisted) β-sheet that is bound to a membrane can be specified by the angle α that the β-sheet makes with the membrane normal, Z, and by the angle β by which the β-strands, c, are tilted within the sheet [36]. Dichroism measurements on the single β-sheet of a small membrane-bound αβ-protein have validated this approach, in that the relative orientations of the β-sheet and α-helices are consistent with the 3-D structure of the protein [40]. Measurement of two dichroic ratios (those of the amide I and amide II bands) is necessary, which requires data for samples dried from H$_2$O and also hydrated in D$_2$O, as in Fig. 4 and Table 3 (see, e.g., refs. [41,42]).

The β-sheet model can be used for a flat β-sandwich, if the angle between the strands in the two sheets is small. Justification for this approximation is given in Appendix A, which presents a detailed analysis for β-sandwiches. The symmetry axis of the β-sandwich is the bisector of the angle between strands in the two sheets, and this is inclined by the angle β to the direction z' in which the β-sandwich is tilted (see Fig. 5). The z'-axis is distributed with axial symmetry about
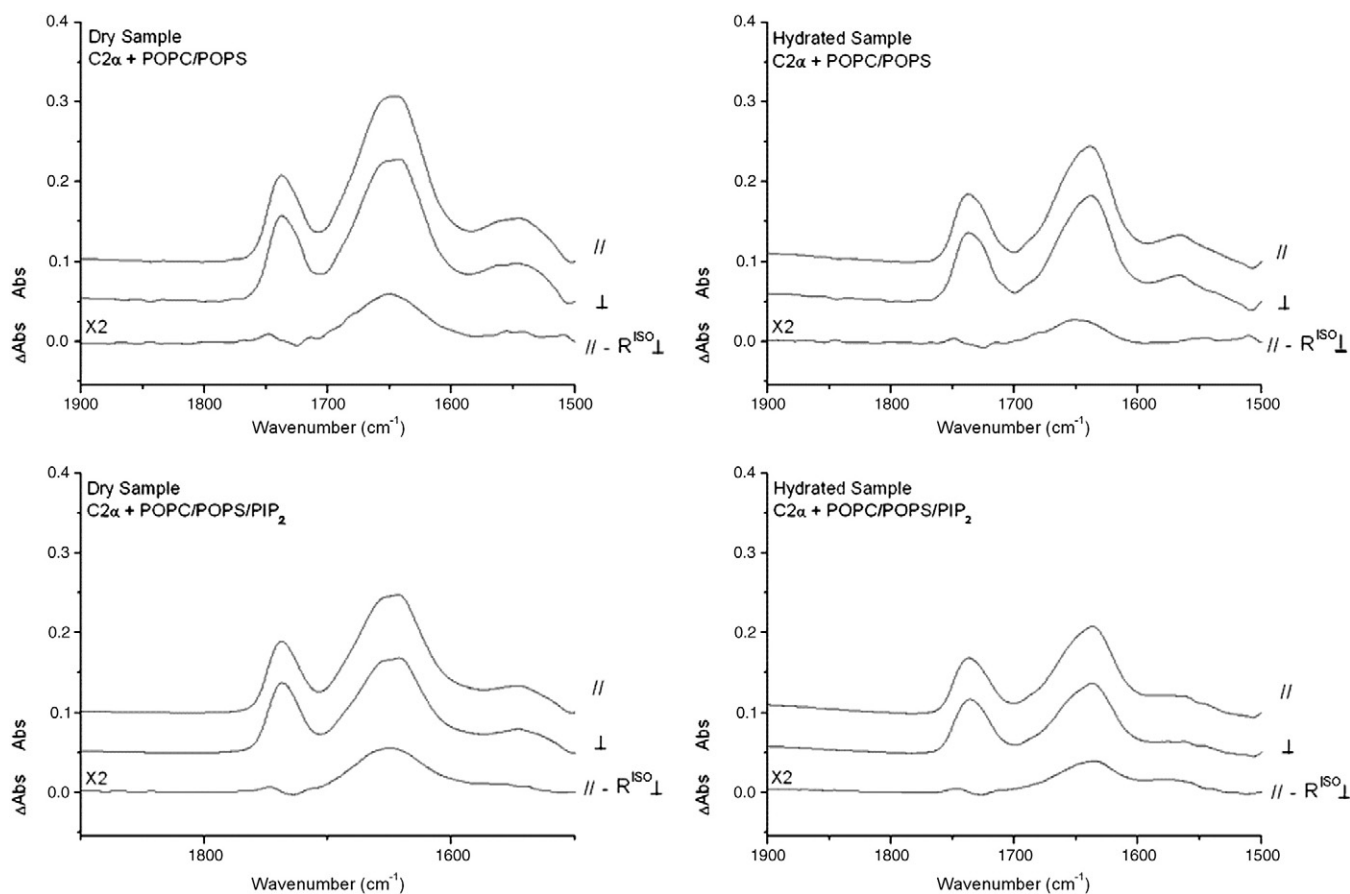

Fig. 4. Amide and carbonyl regions in the ATR-IR spectra from dry (left) and hydrated (right) samples of PKCα-C2 domain in the presence of 75:25 mol/mol POPC/POPS (top) and 70:25:5 mol/mol/mol POPC/POPS/PIP$_2$ (bottom) membranes, for parallel (//, upper spectra) and perpendicular ($\perp$, middle spectra) polarized radiation. The dichroic difference spectra (A$_{//} - R_{iso}A_\perp$, lower spectra) are obtained by subtracting the perpendicular-polarized spectra from the parallel-polarized spectra, after multiplication of the perpendicular-polarized spectra by the dichroic ratio, R_{iso}, appropriate to an isotropic sample distribution. R_{iso} is approximated by the dichroic ratio of the lipid carbonyl band at 1740 cm^{-1} [66]. The spectra are shown in the 1900–1500 cm^{-1} region and are shifted vertically but have the same vertical scale.

Table 3
Dichroic ratios of the principal β-sheet bands in the amide I and amide II bands of the PKCα C2 domain bound to POPC membranes containing 25 mol% POPS or POPA, with and without 5 mol% PIP$_2$, and of the cPLA$_2$ domain bound to POPC/POPS (3:1 mol/mol) membranes.

Dichroic ratios (R) and tilts (α, β)	PKCα-C2 POPC/POPS		PKCα-C2 POPC/POPS/PIP$_2$		PKCα-C2 POPC/POPA		PKCα-C2 POPC/POPA (65:35)		PKCα-C2 POPC/POPA/PIP$_2$		cPLA$_2$-C2 POPC/POPS	
	Dry	Hydrated	Dry	Hydrated	Dry	Hydrated	Dry	Hydrated	Dry	Hydrated	Dry	Hydrated
R$_I$ (main β-sheet band, amide I)	1.780	1.775	1.788	1.583	1.727	1.968	1.676	1.862	1.811	1.589	1.548	1.645
R$_{II}$ (main β-sheet band, amide II)	2.270		1.937		1.672		2.023		1.655		2.426	
$\langle cos^2\beta \rangle$	0.58 ± 0.05		0.54 ± 0.05		0.49 ± 0.01		0.572		0.46 ± 0.02		0.66 ± 0.01	
Angle β (°)	40 ± 3		43 ± 3		46 ± 1		41		47 ± 1		36 ± 1	
$\langle cos^2\alpha \rangle$	0.67 ± 0.05		0.51 ± 0.01		0.64 ± 0.05		0.708		0.45 ± 0.02		0.70 ± 0.05	
Angle α (°)	35 ± 3		44 ± 1		37 ± 3		33		48 ± 1		33 ± 3	

Hydrated data are given for the sample dried down from H$_2$O buffer, and then hydrated with a stream of moist (D$_2$O) air.

the membrane normal. The ATR dichroic ratio of the major amide II band of an antiparallel β-sheet, which has the transition moment oriented parallel to the β-strand axis, is then given by [36]:

$$R_{II} = \frac{E_x^2}{E_y^2} + \frac{2\langle cos^2\alpha\rangle\langle cos^2\beta\rangle}{1-\langle cos^2\alpha\rangle\langle cos^2\beta\rangle}\frac{E_z^2}{E_y^2} \qquad (3)$$

and that of the major amide I band, which has the transition moment oriented perpendicular to the β-strand axis, is given by [36]:

$$R_I = \frac{E_x^2}{E_y^2} + \frac{2\langle cos^2\alpha\rangle\langle sin^2\beta\rangle}{1-\langle cos^2\alpha\rangle\langle sin^2\beta\rangle}\frac{E_z^2}{E_y^2} \qquad (4)$$

where the angular brackets indicate an average over the corresponding orientational distributions. Those in α and in β are uncorrelated.

From the dichroic ratios of the amide I and amide II bands for the dry samples that are given in Table 3, Eqs. (3) and (4) can be combined to obtain the orientations both of the β-strands (i.e., $\langle cos^2\beta\rangle$), and of the β-sandwich (i.e., $\langle cos^2\alpha\rangle$), separately. For a dry sample of the PKCα-C2 domain bound to POPC/POPS membranes, the orientation of the β-strands is: $\langle cos^2\beta\rangle = 0.58$, and that of the β-sandwich is: $\langle cos^2\alpha\rangle = 0.67$. These values are obtained with the thick-film approximation; an essentially identical value of $\langle cos^2\beta\rangle$ is obtained with the thin-film approximation. For the sample hydrated in D$_2$O,
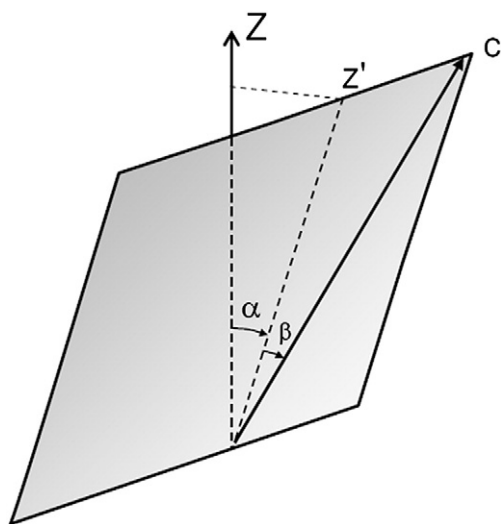

Fig. 5. Orientation of the β-strand axes, *c*, and of the β-sheets in a membrane-associated β-sandwich. The β-sheets are tilted at an angle α to the membrane normal, *Z*. The mean direction of the β-strands is tilted by an angle β in the plane of the sheets. The angle γ of *c* to *Z* is given by Eq. (5), and the azimuthal orientation ϑ of the plane of the sheet about the *c*-axis is given by Eq. (6), where ϑ = 0 is the *Z*,z′-plane. The β-sandwiches (i.e., z′-axes) are distributed with axial symmetry about the membrane normal, *Z* [36].

only the dichroic ratio of the amide I band can be measured. However, it is reasonable to assume that the orientation, $\langle cos^2\beta\rangle = 0.58$, of the β-strands within the sheets does not change appreciably on hydration [34,39]. It is then possible to use Eq. (4), together with the corresponding value of $\langle sin^2\beta\rangle = 1 - \langle cos^2\beta\rangle = 0.42$, to determine the tilt of the β-sandwich. From the dichroic ratio for the hydrated sample of the PKCα-C2 domain bound to POPC/POPS membranes (Table 3), one then obtains: $\langle cos^2\alpha\rangle = 0.67$ by using the thick-film approximation (which should be appropriate to the amount of material used for the sample). This corresponds to an effective tilt of α ≈ 35°, relative to the membrane normal, assuming a single, unique orientation. (Using the thin-film approximation yields $\langle cos^2\alpha\rangle = 0.66$, corresponding to an effective value of α ≈ 36°.)

The lower rows of Table 3 give the results of the above type of docking analysis applied to the PKCα-C2 domain bound to membranes of different lipid compositions, and to the cPLA$_2$-C2 domain bound to POPC/POPS membranes. Changing the membrane lipid composition does not greatly affect the tilt β of the strands within the β-sheet of the PKCα-C2 domain. In particular, the presence of PIP$_2$ in the lipid mixtures does not induce any change in the angle β. More interesting is the effect of PIP$_2$ on the orientation, α, of the PKCα-C2 domain with respect to the membrane normal. As seen above, the value of $\langle cos^2\alpha\rangle$ for the POPC/POPS membrane is about 0.67, which, together with the tilt angle β, corresponds to a docking angle of α = 35 ± 3°. These results do not change greatly with POPA in place of POPS, for which $\langle cos^2\alpha\rangle = 0.64$ and α = 37 ± 3°. However, when PIP$_2$ is present the values of $\langle cos^2\alpha\rangle$ decrease, corresponding to increases of 9° and 11° in the docking angle α for POPC/POPS and POPC/POPA membranes, respectively (see Table 3). This means that, while POPA induces little change in docking angle, the presence of PIP$_2$ causes the PKCα-C2 domain to tilt closer to the membrane surface, irrespective of whether the anionic lipid component is POPA or POPS.

A membrane docking study was also performed with the cPLA$_2$-C2 domain, in order to compare with the PKCα-C2 domain, and also to compare results from the ATR-dichroism method with previous docking data obtained using site-directed spin-labelling [26]. Comparable values for the tilt of the β-strands within the sheet and the tilt of the β-sheets with respect to the membrane normal are obtained for C2 domains from both PKCα and cPLA$_2$. Comparison with spin-label EPR results is given later.

In order to check that the effect of PIP$_2$ on the orientation of the C2 domain is not due just to an increase in the negative charge of the membrane surface, we also used a membrane containing POPC/POPA at 65:35 molar ratio, i.e., containing an additional 10 mol% of POPA. Table 3 shows that the β angle was 41° and the α angle 33°, which is relatively close to the results obtained for a POPC/POPA molar ratio of 75:25 and rather different from those found when PIP$_2$ was present.

In summary, for PKCα-C2 domains and cPLA$_2$-C2 domains docked to membranes not containing PIP$_2$, the plane of the β-sandwich is tilted by effectively α = 34 ± 3° from the membrane normal in hydrated samples, and the mean direction of the β-strands is inclined

by an angle $\beta = 40 \pm 3°$ to the direction of tilt ($36 \pm 1°$ for cPLA2-C_2) (cf. Fig. 5). Note that the crystal structure of the PKCα-C2 domain reveals that the β-strands deviate from their mean direction within the sheet by only $\pm 15°$ (PDB: 1dsy, [8]), which justifies approximating the β-sandwich by a single β-sheet. Explicit calculations, which treat the two sheets separately [46], also support this approximation (see Appendix A).

4. Discussion

The present study utilizes ATR-IR spectroscopy to evaluate the effect of PIP$_2$ on the secondary structure of the PKCα-C2 domain and on docking of the PKCα-C2 domain to lipid membranes. It has been demonstrated extensively that PIP$_2$ interacts with the C2 domains of classical PKCs [14–17,19] and, more recently, the crystal structure of the PKCα-C2 domain in complex with Ca^{2+}, PS and PIP$_2$ has been solved [18]. Nevertheless, the geometry of the domain bound to the membrane, and how the presence of PIP$_2$ affects the docking angle and also the strand tilt within the two sheets, is still not well studied nor understood.

4.1. Secondary structure

Results for the PKCα-C2 domain reveal that binding to different lipid membranes (such as POPC/POPA and POPC/POPS), either containing or lacking PIP$_2$, does not affect the secondary structure, even relative to that in the absence of lipid [54]. This means that when the polybasic cluster of the C2 domain is bound to the membrane by interacting with PIP$_2$, or when POPS is replaced by POPA, the secondary structure remains the same. Only the presence of POPA and PIP$_2$ together may produce some small change, with a decrease in β-sheet population and an increase of β-turns. It was observed previously that the β-sheet content decreases in the presence of negatively charged liposomes composed of POPA alone [22], or a POPC/POPA 20:80 mol/mol mixture [43].

For comparison with the data in Table 1, the secondary structural content deduced from the 3D crystal structure of the PKCα-C2 domain with bound PS and Ca^{2+} (PDB: 1dsy, [8]) is: 46.0% β-strands, 23.4% β-turns, 9.5% helix and 21.2% unassigned, as reported by PROMOTIF v.3.0 [55]. That for the crystal structure with bound PS, Ca^{2+} and PIP$_2$ (PDB: 3gpe, [18]) is: 46.0% β-strands, 22.6% β-turns, 10.2% helix and 21.2% unassigned. The mean values for hydrated membrane-bound samples deduced from ATR spectroscopy are: $55.8 \pm 1.6\%$ β-strands, $22.2 \pm 1.2\%$ β-turns, $11.6 \pm 0.8\%$ α-helix and $10.2 \pm 0.5\%$ unordered. These values are in reasonable accord, when it is allowed that part of the extended chain/β-strand population contributing to the amide I band might remain unassigned in the X-ray structure.

For the NMR solution structure of the cPLA$_2$-C2 domain (PDB code: 1bci [52]), PROMOTIF reports 46.3% β-strands, 25.2% β-turns, 2.4% α-helix and 26.0% unassigned, whereas the PDB header reports 61.7% β-strands (part of which is included by PROMOTIF under β-turns) and 4.1% α-helix. For the crystal structure of the cPLA$_2$-C2 domain (PDB code: 1rlw [56]), PROMOTIF reports 50.8% β-strands, 24.6% β-turns, 7.1% helix and 17.5% unassigned, and the PDB header reports 46.8% β-strands and 7.1% helix. The values for hydrated membrane-bound cPLA$_2$-C2 domain deduced from ATR spectroscopy are: 47% β-strands, 19% β-turns, 5% α-helix and 13% unordered, plus 16% corresponding to the β-edge band at 1626 cm^{-1} (see Table 1). To within the uncertainties in the estimates from the NMR structure and attribution of the β-edge band, the two sets of spectroscopic measurements on the hydrated protein are in reasonable accord.

4.2. ATR-dichroism to study docking of C2 domains

ATR-IR spectroscopy has been used widely for studies of phospholipid membranes and molecules interacting with lipid bilayers. At present, use of ATR-IR to study the orientation or docking of peptides or proteins in membranes has been confined mostly to α-helix, β-sheet or β-barrel structures (see, e.g., refs. [28,30,31,36–42]). In the present study, a β-sheet model is applied to the C2 domain β-sandwich by considering two sheets parallel to one other. This extended model that is given in Appendix A can be applied to many β-sandwich structures with a good degree of approximation, because it takes into account not only the inclination, α, of the β-sheets to the membrane normal and the tilt, β, of the β-strands within the sheet, but also the angle, 2ε, between the strands in the two sheets of the β-sandwich. Possibly, a more complicated analysis may be required for sandwiches where the two sheets are not parallel, but this is not the case for the C2 domain of PKCα [8].

Docking studies with site-directed spin-labelling have been used previously to determine the orientation of PKCα-C2 and two other C2 domains when bound to lipid membranes [24–26]. Very recently, also X-ray reflectivity has been used to investigate docking of the PKCα-C2 domain on monolayers containing anionic lipids [27]. In these studies, the domain orientation was characterised by the net tilt, γ, of the β-strands from the bilayer normal and the azimuthal orientation, ϑ, of the sheets about the strand axis, *c* (see Fig. 5). In terms of the angles α and β that are used to characterise the IR-dichroism, the strand tilt is given by [36]:

$$cos\gamma = cos\alpha \, cos\beta \tag{5}$$

which yields a value of $\gamma \approx 51 \pm 4°$ from the IR data for the PKCα-C2 domain. This can be compared with tilts of $\gamma = 68 \pm 7°$ and $35 \pm 10°$ that are obtained from the docking studies with site-directed spin labels [57,58] and with X-ray reflectivity measurements on monolayers [27], respectively. The strand tilt deduced from IR-dichroism, which measures angular orientation directly, lies between the two extremes. The second angular parameter, the azimuthal orientation, ϑ, of the sheets about the strand axis, *c*, is given by [36]:

$$cos\vartheta = tan\beta \, / \, tan\gamma. \tag{6}$$

This azimuthal angle ϑ is referred to the normal to the β-sheet and is the complement of the angle φ that is used by Malmberg et al. [26] to specify the sheet orientation, i.e., $\phi = 90° - \vartheta$ (see Fig. 5). (The azimuthal angle used by Chen et al. [27] in analysing X-ray reflectivity is reported as $360° - \phi$.)

Table 4 compares the present results from IR-dichroism with those from site-directed spin-labelling and X-ray reflectivity by transforming data from the latter with Eqs. (5) and (6). ATR-dichroism provides a direct measure of the angular orientation, whereas site-directed spin-labelling techniques and X-ray reflectivity provide depth-dependent measurements from which angular information comes indirectly via docking trials with a known protein structure. This is reflected in the relatively large angular uncertainties from reflectivity

Table 4
Orientation of β-sheets and β-strands in C2 domains docked to membranes.[a]

Protein	α (°)	β (°)	Ref.
PKCα	35 ± 3	40 ± 3	This work
	25 ± 6[b]	76 ± 8[b]	[24,26]
	30 ± 15	20 ± 20	[27]
cPLA$_2$	33 ± 3	36 ± 1	This work
	28 ± 6	46 ± 7	[26]
SytIA	0 ± 5	71 ± 5	[68,26]

[a] For definition of α and β, see Fig. 5. Values obtained in this work from IR-dichroism are compared with calculations from docking studies with site-directed spin-labelling that are reported in refs. [26,58,57], and with X-ray reflectivity in ref. [27], by using Eqs. (5) and (6).
[b] The EPR results for PKCα-C2 are from a smaller dataset which yields a larger strand tilt ($\gamma = 77°$ [24]) than that obtained with a more extensive dataset [57,58] for which the azimuthal orientation is not available.

measurements with the PKCα-C2 domain. These encompass the direct angular determinations from IR-dichroism but – as already pointed out by Chen et al. [27] – not the indirect inferences from site-directed EPR. The latter also are not consistent with the direct determinations from IR-dichroism. Whereas EPR-relaxation enhancements within the membrane are well established in site-directed EPR by calibration with spin-labelled lipid chains [59,60], those outside the membrane rely on uncertain extrapolations that rapidly become insensitive to position in the aqueous phase. Exactly the latter are required for site-directed spin-labelling of the PKCα-C2 domain, which does not penetrate the hydrophobic core on binding to lipid membranes. This accounts for the lack of agreement between the orientation of the PKCα-C2 domain deduced from site-directed spin-labelling and that deduced from IR-dichroism (and X-ray reflectivity). In support of this interpretation is that the orientation deduced from site-directed EPR for the cytosolic phospholipase A$_2$ (cPLA$_2$) C2 domain, which penetrates the hydrophobic region of the membrane, agrees far better with the direct determination from IR-dichroism than does that from the non-penetrant PKCα-C2 domain.

Regarding the comparison between IR-dichroism and site-directed spin-labelling, it should be noted that somewhat different criteria are used to define the orientation of the β-strands and β-sheets in the two cases. Of necessity, the IR method provides values which are averaged over all amides of the peptide chain that are involved in β-strands. On the other hand, to facilitate intercomparison between different C2 domains, orientations deduced from docking with site-directed spin-labelling were defined by just three C$^\alpha$ positions in one β-sheet. These were chosen to be at the ends of the longest β-strand and at an intermediate position in an adjacent strand; equivalent residues were chosen in all three C2 domains that are compared in Table 4. Thus deviations between the two sets of values might arise from non-planarity of the β-sheets. The two sheets of the β-sandwich are closely parallel [8], which otherwise might also contribute to differences, but the non-colinearity of the strands has little effect on the IR result, as is shown in Appendix A.

In its simplest form, IR-dichroism of the amide I and amide II bands from β-sandwich proteins has the advantage, relative to site-directed spin-labelling studies with paramagnetic relaxants [24,57], that it involves considerably fewer measurements and does not require site-directed cysteine mutants. As regards membrane-bound C2 domains, it also has greater orientational sensitivity because concentration gradients of paramagnetic relaxants are rather small for surface-associated proteins [26,57]. However, IR-dichroism gives only orientational data on surface docking, and provides no information on the vertical location of the protein relative to the membrane, which is the principal strength of both site-directed EPR and X-ray reflectivity. Ideally, the constraints on orientation from IR-dichroism could be used in the optimisation procedure to provide further refinement when fitting the depth parameters from site-directed spin-labelling, or X-ray reflectivity.

4.3. Role of PIP$_2$ in membrane docking of C2 domains

One of the main purposes of this work is to understand the role of the polybasic cluster of the PKCα-C2 domain in its docking to membranes. Recent structural studies have revealed that the C2 domain of PKCα possesses a binding site on the concave surface of the β-strands (mainly strands β3 and β4), which is highly specific for PIP$_2$ [18]. This motif binds PIP$_2$ with very high specificity [16,18,19]. It is found here that, whereas substitution of the anionic lipid POPS by POPA produces only small change in orientation of the PKCα-C2 domain (see Table 3), introduction of the specific lipid PIP$_2$ has a pronounced effect on the orientation of the membrane-bound C2 domain (see Table 3), whilst leaving lipid chain order unaffected (see Table 2). With respect to this role of PIP$_2$ in membrane docking, it should be emphasized that similar enhancements in tilt are obtained

with two independent anionic lipid systems, POPC/POPS and POPC/POPA, although the absolute tilt angles differ slightly.

Fig. 6A and B illustrates the two possible dockings of the PKCα-C2 domain to the membrane in a configuration that takes account of the results from IR-dichroism. Both are characterised by a tilt of α = 35° between the plane of the β-sheets and the normal to the plane of the membrane. In the two cases, the C2 domain binds to POPC/POPS by using the Ca^{2+}-binding region at the top of the β-sandwich, with loops 1 and 3 establishing a number of interactions with the phospholipids. The difference between the two alternatives resides in the penetration of each loop into the membrane interface. In Fig. 6A, loop 1 penetrates more than does loop 3, and the opposite situation is represented by Fig. 6B, where loop 3 penetrates more than does loop 1. Several mutagenesis studies have demonstrated that substitution of critical residues in loop 1 is less deleterious to both membrane binding and catalytic activity [7,10,61] than is that of residues located in loop 3. These results are consistent with the model represented in Fig. 6B, which places Arg249 and Thr251 (loop 3) within the phospholipid headgroup region and Asn189 and Arg216 (loop 1) in a more superficial location.

The docking orientation changes from that shown in Fig. 6A and B for POPC/POPS to that in Fig. 6C when PIP$_2$ is present in the membrane. This corresponds to an increase from 35° to 44° in the angle α which the β-sheets of the C2 domain make with the membrane normal. PIP$_2$ therefore enhances anchoring of the domain such that the β-sandwich approaches closer to the membrane surface, in qualitative agreement with the results of site-directed EPR [25], and thus becomes more stably bound (see [62]). This occurs by the interactions that PIP$_2$ establishes with its specific site in the β-groove, which is located in the lateral part of the C2 domain and is composed of the residues Lys197, Tyr195, Lys209, Lys211, Trp245 and Asn253 [18].

It is found that the inositol ring of PI is oriented perpendicular to the bilayer surface [63], and phosphorylation at C4 and C5 of the ring induces a bend toward the bilayer surface [63,64]. This orientation of the inositol ring is that required by the crystal structure to facilitate docking of the PIP$_2$-bound C2 domain at the membrane surface [18]. In addition, this orientation also allows PtdIns(3,4,5)P$_3$ to bind to the C2 domain (as it does, with lower affinity [19,23,65]), because the phosphate at C3 of the inositol ring points to the membrane interface and is not involved in interaction with the protein. Note that Fig. 6 is a modelling study; it represents the specific docking of POPS and PIP$_2$ to the protein but does not refer to an explicit mole fraction of the ionic lipids. In general, it is expected that the negatively charged lipids are recruited to the protein binding site as a result of their affinity for the protein (see, e.g., ref. [66]).

In summary, this work introduces a new means to study the membrane docking of C2 domains, and other domains that contain a β-sandwich fold, by using ATR-IR-dichroism. The results reported here are consistent with previous structural results and clearly indicate that the interaction with PIP$_2$ facilitates a closer contact of the C2 domain with the membrane and this probably facilitates the activation of PKCα.

Appendix A. Mutually tilted strands in β-sandwiches

For a flat β-sandwich, where the angle between the strands in the two sheets is 2ε, the strands are tilted by an angle β ± ε, in sheets A

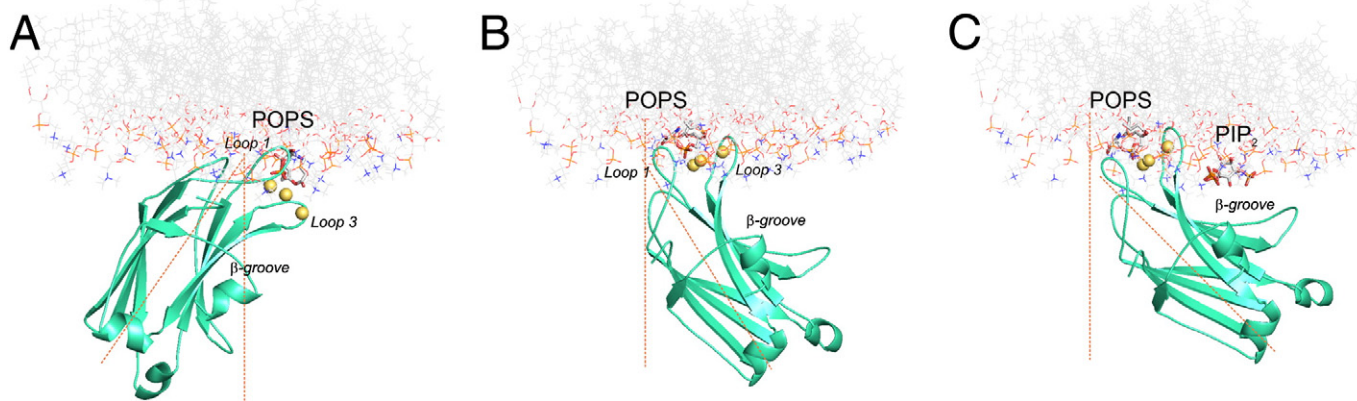**Fig. 6.** C2 domain of PKCα docked to the surface of membranes without (A and B) and with (C) PIP$_2$. The C2 domain of PKCα is represented as a ribbon model in green by using the PDB codes (A and B) 1dsy [8] and (C) 3gpe [18]. The lipid membrane corresponds to a POPC molecular dynamics simulation (popc128a) [68] and is represented as a stick model with carbon in grey, nitrogen in blue and oxygen in red. The head groups of the two anionic phospholipids, phosphatidylserine (POPS) and PIP$_2$ led us to dock the domain in the hydrophilic region of the membrane bilayer. To orientate the tilt of the domain with respect to the normal to the membrane surface, we used α angles $35\pm3°$ (A and B) and $44\pm1°$ (C) obtained from the ATR-IR measurements with POPC/POPS$\pm$PIP$_2$. Figure prepared with PyMOL (DeLano Scientific LLC, San Francisco).

and B, respectively (see Fig. 7). As before, β is the tilt of the symmetry axis of the β-strands within the plane of the β-sandwich.

The dichroic ratio of the amide II band for sheet A in the β-sandwich is therefore given from Eq. (3) by:

$$R_{II,A} = \frac{E_x^2}{E_y^2} + \frac{2\langle cos^2\alpha\rangle\langle cos^2(\beta+\varepsilon)\rangle}{1-\langle cos^2\alpha\rangle\langle cos^2(\beta+\varepsilon)\rangle}\frac{E_z^2}{E_y^2} \quad (A.1)$$

and that for sheet B is given by:

$$R_{II,B} = \frac{E_x^2}{E_y^2} + \frac{2\langle cos^2\alpha\rangle\langle cos^2(\beta-\varepsilon)\rangle}{1-\langle cos^2\alpha\rangle\langle cos^2(\beta-\varepsilon)\rangle}\frac{E_z^2}{E_y^2}. \quad (A.2)$$

Correspondingly, the dichroic ratio of the amide I band for sheet A in the β-sandwich is given from Eq. (4) by:

$$R_{I,A} = \frac{E_x^2}{E_y^2} + \frac{2\langle cos^2\alpha\rangle\langle sin^2(\beta+\varepsilon)\rangle}{1-\langle cos^2\alpha\rangle\langle sin^2(\beta+\varepsilon)\rangle}\frac{E_z^2}{E_y^2} \quad (A.3)$$
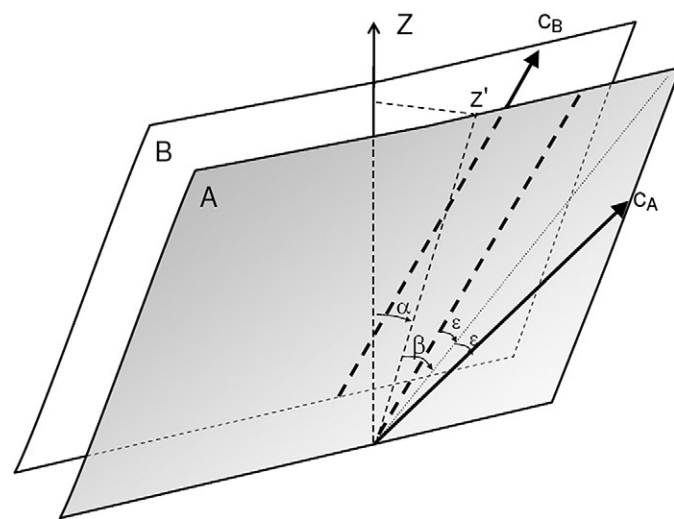

Fig. 7. Relative orientation, $\pm\varepsilon$, of the β-strand axes, c_A and c_B, in β-sheets A and B of a membrane-associated β-sandwich. The mean direction of the β-strands is tilted by an angle β in the plane of the sheets, and the strands themselves are tilted by $\beta\pm\varepsilon$ in the two sheets (cf. Fig. 5).

and that for sheet B is given by:

$$R_{I,B} = \frac{E_x^2}{E_y^2} + \frac{2\langle cos^2\alpha\rangle\langle sin^2(\beta-\varepsilon)\rangle}{1-\langle cos^2\alpha\rangle\langle sin^2(\beta-\varepsilon)\rangle}\frac{E_z^2}{E_y^2} \quad (A.4)$$

where angular brackets again indicate an average over the corresponding orientational distributions. Those in α and in β (and ε) are uncorrelated.

The dichroism of the complete β-sandwich (either amide I or amide II band) is given by the ratio of the weighted absorption intensities for parallel and perpendicularly polarized radiation. If f_A is the fractional intensity contributed by sheet A (where $f_A+f_B=1$), then taking into account the geometry of the ATR setup, the dichroism of the entire β-sandwich is given by [46]:

$$R = \frac{R_B+G}{1-f_A(R_A-R_B)/(R_A+G)}-G \quad (A.5)$$

where $G=(2E_z^2-E_x^2)/E_y^2$. For the amide II band: $R_A\equiv R_{II,A}$ and $R_B\equiv R_{II,B}$ in Eq. (A.5), and equivalently for the amide I band.

The relative orientation of the β-strands in the sandwich: $2\varepsilon=31°$, and the relative size of the two sheets: $f_A\approx0.5$, are known from the crystal structure (PDB: 1dsy, [8]). From the dichroic ratios of the amide I and amide II bands for the dry sample in Table 3, Eqs. (A.1) to (A.5) then give the orientation of the β-strands as: $\beta=40\pm3°$, and of the β-sandwich as: $\langle cos^2\alpha\rangle=0.67$, with the thick-film approximation. The value of β is very close to that obtained from the approximation using Eqs. (3) and (4), and that for $\langle cos^2\alpha\rangle$ is identical. From the dichroic ratio of the amide I band for the hydrated sample in Table 3, and the fixed tilt $\beta=40\pm3°$ of the β-strands within the sheets, one obtains: $\langle cos^2\alpha\rangle=0.67$ from Eqs. (4) to (6) by using the thick-film approximation. This corresponds to an effective tilt of $\alpha=35\pm3°$, relative to the membrane normal, which again is identical to the value obtained with the approximation given by Eqs. (3) and (4).

References

[1] Y. Nishizuka, The molecular heterogeneity of protein kinase C and its implications for cellular regulation, Nature 334 (1988) 661–665.
[2] A.C. Newton, Protein kinase C: structure, function, and regulation, J. Biol. Chem. 270 (1995) 28495–28498.
[3] S. Corbalan-Garcia, J.C. Gomez-Fernandez, Protein kinase C regulatory domains: the art of decoding many different signals in membranes, Biochim. Biophys. Acta 1761 (2006) 633–654.
[4] H. Mellor, P.J. Parker, The extended protein kinase C superfamily, Biochem. J. 332 (Pt 2) (1998) 281–292.

[5] J. Hofmann, The potential for isoenzyme-selective modulation of protein kinase C, FASEB J. 11 (1997) 649–669.

[6] W. Cho, R.V. Stahelin, Membrane binding and subcellular targeting of C2 domains, Biochim. Biophys. Acta 1761 (2006) 838–849.

[7] P. Conesa-Zamora, M.J. Lopez-Andreo, J.C. Gomez-Fernandez, S. Corbalan-Garcia, Identification of the phosphatidylserine binding site in the C2 domain that is important for PKCα activation and *in vivo* cell localization, Biochemistry 40 (2001) 13898–13905.

[8] N. Verdaguer, S. Corbalan-Garcia, W.F. Ochoa, I. Fita, J.C. Gomez-Fernandez, Ca^{2+} bridges the C2 membrane-binding domain of protein kinase Cα directly to phosphatidylserine, EMBO J. 18 (1999) 6329–6338.

[9] W.F. Ochoa, S. Corbalan-Garcia, R. Eritja, J.A. Rodriguez-Alfaro, J.C. Gomez-Fernandez, I. Fita, N. Verdaguer, Additional binding sites for anionic phospholipids and calcium ions in the crystal structures of complexes of the C2 domain of protein kinase Cα, J. Mol. Biol. 320 (2002) 277–291.

[10] S.R. Bolsover, J.C. Gomez-Fernandez, S. Corbalan-Garcia, Role of the Ca^{2+}/phosphatidylserine binding region of the C2 domain in the translocation of protein kinase Cα to the plasma membrane, J. Biol. Chem. 278 (2003) 10282–10290.

[11] S. Corbalan-Garcia, J.A. Rodriguez-Alfaro, J.C. Gomez-Fernandez, Determination of the calcium-binding sites of the C2 domain of protein kinase Cα that are critical for its translocation to the plasma membrane, Biochem. J. 337 (Pt 3) (1999) 513–521.

[12] J.A. Rodriguez-Alfaro, J.C. Gomez-Fernandez, S. Corbalan-Garcia, Role of the lysine-rich cluster of the C2 domain in the phosphatidylserine-dependent activation of PKCα, J. Mol. Biol. 335 (2004) 1117–1129.

[13] W.F. Ochoa, A. Torrecillas, I. Fita, N. Verdaguer, S. Corbalan-Garcia, J.C. Gomez-Fernandez, Retinoic acid binds to the C2-domain of protein kinase Cα, Biochemistry 42 (2003) 8774–8779.

[14] S. Corbalan-Garcia, J. Garcia-Garcia, J.A. Rodriguez-Alfaro, J.C. Gomez-Fernandez, A new phosphatidylinositol 4, 5-bisphosphate-binding site located in the C2 domain of protein kinase Cα, J. Biol. Chem. 278 (2003) 4972–4980.

[15] C. Marin-Vicente, J.C. Gomez-Fernandez, S. Corbalan-Garcia, The ATP-dependent membrane localization of protein kinase Cα is regulated by Ca^{2+} influx and phosphatidylinositol 4, 5-bisphosphate in differentiated PC12 cells, Mol. Biol. Cell 16 (2005) 2848–2861.

[16] S. Sanchez-Bautista, C. Marin-Vicente, J.C. Gomez-Fernandez, S. Corbalan-Garcia, The C2 domain of PKCα is a Ca^{2+}-dependent PtdIns(4, 5)P2 sensing domain: a new insight into an old pathway, J. Mol. Biol. 362 (2006) 901–914.

[17] J.H. Evans, D. Murray, C.C. Leslie, J.J. Falke, Specific translocation of protein kinase Cα to the plasma membrane requires both Ca^{2+} and PIP$_2$ recognition by its C2 domain, Mol. Biol. Cell 17 (2006) 56–66.

[18] M. Guerrero-Valero, C. Ferrer-Orta, J. Querol-Audi, C. Marin-Vicente, I. Fita, J.C. Gomez-Fernandez, N. Verdaguer, S. Corbalan-Garcia, Structural and mechanistic insights into the association of PKCα-C2 domain to PtdIns(4, 5)P2, Proc. Natl Acad. Sci. USA 106 (2009) 6603–6607.

[19] M. Guerrero-Valero, C. Marin-Vicente, J.C. Gomez-Fernandez, S. Corbalan-Garcia, The C2 domains of classical PKCs are specific PtdIns(4, 5)P2-sensing domains with different affinities for membrane binding, J. Mol. Biol. 371 (2007) 608–621.

[20] C. Marin-Vicente, F.E. Nicolas, J.C. Gomez-Fernandez, S. Corbalan-Garcia, The PtdIns(4, 5)P2 ligand itself influences the localization of PKCα in the plasma membrane of intact living cells, J. Mol. Biol. 377 (2008) 1038–1052.

[21] P. Conesa-Zamora, J.C. Gomez-Fernandez, S. Corbalan-Garcia, The C2 domain of protein kinase Cα is directly involved in the diacylglycerol-dependent binding of the C1 domain to the membrane, Biochim. Biophys. Acta 1487 (2000) 246–254.

[22] J. Garcia-Garcia, S. Corbalan-Garcia, J.C. Gomez-Fernandez, Effect of calcium and phosphatidic acid binding on the C2 domain of PKCα as studied by Fourier transform infrared spectroscopy, Biochemistry 38 (1999) 9667–9675.

[23] D. Manna, N. Bhardwaj, M.S. Vora, R.V. Stahelin, H. Lu, W. Cho, Differential roles of phosphatidylserine, PtdIns(4, 5)P2, and PtdIns(3, 4, 5)P3 in plasma membrane targeting of C2 domains. Molecular dynamics simulation, membrane binding, and cell translocation studies of the PKCα C2 domain, J. Biol. Chem. 283 (2008) 26047–26058.

[24] S.C. Kohout, S. Corbalan-Garcia, J.C. Gomez-Fernandez, J.J. Falke, C2 domain of protein kinase Cα: elucidation of the membrane docking surface by site-directed fluorescence and spin labeling, Biochemistry 42 (2003) 1254–1265.

[25] K.E. Landgraf, N.J. Malmberg, J.J. Falke, Effect of PIP$_2$ binding on the membrane docking geometry of PKCα C2 domain: an EPR site-directed spin-labeling and relaxation study, Biochemistry 47 (2008) 8301–8316.

[26] N.J. Malmberg, D.R. Van Buskirk, J.J. Falke, Membrane-docking loops of the cPLA2 C2 domain: detailed structural analysis of the protein–membrane interface via site-directed spin-labeling, Biochemistry 42 (2003) 13227–13240.

[27] C.H. Chen, S. Malkova, S.V. Pingali, F. Long, S. Garde, W. Cho, M.L. Schlossman, Configuration of PKCα-C2 domain bound to mixed SOPC/SOPS lipid monolayers, Biophys. J. 97 (2009) 2794–2802.

[28] D. Marsh, Spin-label electron spin resonance and Fourier transform infrared spectroscopy for structural/dynamic measurements on ion channels, Methods Enzymol. 294 (1999) 59–92.

[29] A. Ausili, A. Torrecillas, M.M. Martinez-Senac, S. Corbalan-Garcia, J.C. Gomez-Fernandez, The interaction of the Bax C-terminal domain with negatively charged lipids modifies the secondary structure and changes its way of insertion into membranes, J. Struct. Biol. 164 (2008) 146–152.

[30] Z. Kota, T. Pali, N. Dixon, T.P. Kee, M.A. Harrison, J.B. Findlay, M.E. Finbow, D. Marsh, Incorporation of transmembrane peptides from the vacuolar H$^+$-ATPase in phospholipid membranes: spin-label electron paramagnetic resonance and polarized infrared spectroscopy, Biochemistry 47 (2008) 3937–3949.

[31] D. Marsh, Orientation and peptide–lipid interactions of alamethicin incorporated in phospholipid membranes: polarized infrared and spin-label EPR spectroscopy, Biochemistry 48 (2009) 729–737.

[32] D. Marsh, T. Pali, Infrared dichroism from the X-ray structure of bacteriorhodopsin, Biophys. J. 80 (2001) 305–312.

[33] D. Marsh, M. Muller, F.J. Schmitt, Orientation of the infrared transition moments for an α-helix, Biophys. J. 78 (2000) 2499–2510.

[34] T. Pali, D. Marsh, Tilt, twist, and coiling in β-barrel membrane proteins: relation to infrared dichroism, Biophys. J. 80 (2001) 2789–2797.

[35] D. Marsh, Infrared dichroism of twisted β-sheet barrels. The structure of E. coli outer membrane proteins, J. Mol. Biol. 297 (2000) 803–808.

[36] D. Marsh, Dichroic ratios in polarized Fourier transform infrared for nonaxial symmetry of β-sheet structures, Biophys. J. 72 (1997) 2710–2718.

[37] D. Marsh, Nonaxiality in infrared dichroic ratios of polytopic transmembrane proteins, Biophys. J. 75 (1998) 354–358.

[38] D. Marsh, Infrared dichroism of isotope-edited α-helices and β-sheets, J. Mol. Biol. 338 (2004) 353–367.

[39] M. Ramakrishnan, J. Qu, C.L. Pocanschi, J.H. Kleinschmidt, D. Marsh, Orientation of β-barrel proteins OmpA and FhuA in lipid membranes. Chain length dependence from infrared dichroism, Biochemistry 44 (2005) 3515–3523.

[40] J.A. Richard, I. Kelly, D. Marion, M. Pezolet, M. Auger, Interaction between β-Purothionin and dimyristoylphosphatidylglycerol: a (31)P-NMR and infrared spectroscopic study, Biophys. J. 83 (2002) 2074–2083.

[41] V. Anbazhagan, J. Qu, J.H. Kleinschmidt, D. Marsh, Incorporation of outer membrane protein OmpG in lipid membranes: protein–lipid interactions and β-barrel orientation, Biochemistry 47 (2008) 6189–6198.

[42] V. Anbazhagan, N. Vijay, J.H. Kleinschmidt, D. Marsh, Protein–lipid interactions with Fusobacterium nucleatum major outer membrane protein FomA: spin-label EPR and polarized infrared spectroscopy, Biochemistry 47 (2008) 8414–8423.

[43] A. Torrecillas, S. Corbalan-Garcia, J.C. Gomez-Fernandez, Structural study of the C2 domains of the classical PKC isoenzymes using infrared spectroscopy and two-dimensional infrared correlation spectroscopy, Biochemistry 42 (2003) 11669–11681.

[44] E.A. Nalefski, T. McDonagh, W. Somers, J. Seehra, J.J. Falke, J.D. Clark, Independent folding and ligand specificity of the C2 calcium-dependent lipid binding domain of cytosolic phospholipase A2, J. Biol. Chem. 273 (1998) 1365–1372.

[45] U.P. Fringeli, H.H. Gunthard, Infrared membrane spectroscopy, Mol. Biol. Biochem. Biophys. 31 (1981) 270–332.

[46] D. Marsh, Quantitation of secondary structure in ATR infrared spectroscopy, Biophys. J. 77 (1999) 2630–2637.

[47] S.C. Kohout, S. Corbalan-Garcia, A. Torrecillas, J.C. Gomez-Fernandez, J.J. Falke, C2 domains of protein kinase C isoforms α, β, and γ: activation parameters and calcium stoichiometries of the membrane-bound state, Biochemistry 41 (2002) 11411–11424.

[48] J.L. Arrondo, A. Muga, J. Castresana, F.M. Goni, Quantitative studies of the structure of proteins in solution by Fourier-transform infrared spectroscopy, Prog. Biophys. Mol. Biol. 59 (1993) 23–56.

[49] S. Krimm, J. Bandekar, Vibrational spectroscopy and conformation of peptides, polypeptides, and proteins, Adv. Protein Chem. 38 (1986) 181–364.

[50] A. Barth, The infrared absorption of amino acid side chains, Prog. Biophys. Mol. Biol. 74 (2000) 141–173.

[51] W.K. Surewicz, H.H. Mantsch, New insight into protein secondary structure from resolution-enhanced infrared spectra, Biochim. Biophys. Acta 952 (1988) 115–130.

[52] G.Y. Xu, T. McDonagh, H.A. Yu, E.A. Nalefski, J.D. Clark, D.A. Cumming, Solution structure and membrane interactions of the C2 domain of cytosolic phospholipase A2, J. Mol. Biol. 280 (1998) 485–500.

[53] E. Goormaghtigh, V. Raussens, J.M. Ruysschaert, Attenuated total reflection infrared spectroscopy of proteins and lipids in biological membranes, Biochim. Biophys. Acta 1422 (1999) 105–185.

[54] A. Torrecillas, M.M. Martinez-Senac, E. Goormaghtigh, A. de Godos, S. Corbalan-Garcia, J.C. Gomez-Fernandez, Modulation of the membrane orientation and secondary structure of the C-terminal domains of Bak and Bcl-2 by lipids, Biochemistry 44 (2005) 10796–10809.

[55] E.G. Hutchinson, J.M. Thornton, PROMOTIF — a program to identify and analyze structural motifs in proteins, Protein Sci. 5 (1996) 212–220.

[56] O. Perisic, S. Fong, D.E. Lynch, M. Bycroft, R.L. Williams, Crystal structure of a calcium–phospholipid binding domain from cytosolic phospholipase A2, J. Biol. Chem. 273 (1998) 1596–1604.

[57] N.J. Malmberg, J.J. Falke, Use of EPR power saturation to analyze the membrane-docking geometries of peripheral proteins: applications to C2 domains, Annu. Rev. Biophys. Biomol. Struct. 34 (2005) 71–90.

[58] N.J. Malmberg, Spectroscopic characterization of membrane docking C2 domains, University of Colorado, Boulder, 2004, p. 167.

[59] B.G. Dzikovski, V.A. Livshits, D. Marsh, Oxygen permeation profile in lipid membranes: comparison with transmembrane polarity profile, Biophys. J. 85 (2003) 1005–1012.

[60] D. Marsh, B.G. Dzikovski, V.A. Livshits, Oxygen profiles in membranes, Biophys. J. 90 (2006) L49–L51.

[61] R.V. Stahelin, J.D. Rafter, S. Das, W. Cho, The molecular basis of differential subcellular localization of C2 domains of protein kinase C-α and group IVa cytosolic phospholipase A2, J. Biol. Chem. 278 (2003) 12452–12460.

[62] J.A. Corbin, J.H. Evans, K.E. Landgraf, J.J. Falke, Mechanism of specific membrane targeting by C2 domains: localized pools of target lipids enhance Ca^{2+} affinity, Biochemistry 46 (2007) 4322–4336.

[63] J.P. Bradshaw, R.J. Bushby, C.C. Giles, M.R. Saunders, Orientation of the headgroup of phosphatidylinositol in a model biomembrane as determined by neutron diffraction, Biochemistry 38 (1999) 8393–8401.

[64] A.I. Kishore, J.H. Prestegard, Molecular orientation and conformation of phosphatidylinositides in membrane mimetics using variable angle sample spinning (VASS) NMR, Biophys. J. 85 (2003) 3848–3857.

[65] R.B. Sutton, S.R. Sprang, Structure of the protein kinase Cβ phospholipid-binding C2 domain complexed with Ca^{2+}, Structure 6 (1998) 1395–1405.

[66] T. Heimburg, B. Angerstein, D. Marsh, Binding of peripheral proteins to mixed lipid membranes: effect of lipid demixing upon binding, Biophys. J. 76 (1999) 2575–2586.

[67] B. Bechinger, J.M. Ruysschaert, E. Goormaghtigh, Membrane helix orientation from linear dichroism of infrared attenuated total reflection spectra, Biophys. J. 76 (1999) 552–563.

[68] B. Hoff, E. Strandberg, A.S. Ulrich, D.P. Tieleman, C. Posten, ^{2}H-NMR study and molecular dynamics simulation of the location, alignment, and mobility of pyrene in POPC bilayers, Biophys. J. 88 (2005) 1818–1827.